ACS Catalysis

Research Article

pubs.acs.org/acscatalysis

Cu-Deficient Plasmonic $Cu_{2-x}S$ Nanoplate Electrocatalysts for Oxygen Reduction

Xianliang Wang, Yujie Ke, Hengyu Pan, Kuo Ma, Qinqin Xiao, Deqiang Yin, Gang Wu,* and Mark T. Swihart*

Department of Chemical and Biological Engineering, University at Buffalo (SUNY), Buffalo, New York 14260-4200, United States

Supporting Information

ABSTRACT: Cation deficient transition metal sulfides have attracted increased attention due to their unique properties that arise from degenerate *p*-doping, particularly their localized surface plasmon resonance (LSPR) and related optical properties. Here, we present the first study of their electrocatalytic activity. We developed a facile one-pot method to prepare *p*-doped copper sulfide nanoplates with tunable LSPR at moderate temperature (below 100 °C) without any hot injection or rapid mixing step. The doping level was controlled by varying the concentration of cation precursor (Cu^{2+}) to finely tune the LSPR wavelength without changing the nanoplate size or morphology. $Cu_{2-x}S$ nanoplates with three different doping levels were tested for their electrocatalytic activity for the oxygen reduction reaction (ORR) in alkaline solution. Importantly, increasing the concentration of free holes in $Cu_{2-x}S$ significantly enhanced the ORR catalytic activity. Furthermore, to improve the electrical conductivity, the most heavily doped $Cu_{2-x}S$ nanoplates were deposited on carbon black (Vulcan XC-72) and reduced graphene oxide (rGO), thereby leading to substantial enhancement of ORR steady-state current in both electrochemical and mass-transfer controlled potential regions. A calculation of average electron transfer number along with the measured peroxide yield indicated that both carbon black and rGO supported $Cu_{2-x}S$ catalysts can provide a four-electron reduction pathway. The ORR catalytic activity of the $Cu_{2-x}S$ nanoplates does not yet match that of state-of-the-art Pt/C catalysts. However, this work opens up new opportunities to apply *p*-doped copper chalcogenides as electrocatalysts for the ORR beyond conventional nonprecious metal catalysts based upon Fe, Co, N, and C.

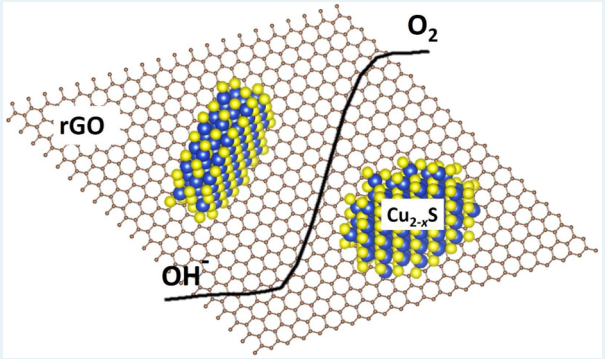

KEYWORDS: *colloidal synthesis, localized surface plasmon resonance, oxygen reduction reaction, electrocatalyst, reduced graphene oxide, copper sulfide*

INTRODUCTION

Copper chalcogenides (Cu_xE with E = S, Se, or Te and *x* from 1 to 2) with bandgap energies of 1.0−1.5 eV have been drawing increasing attention due to their unique properties and potential applications in low-cost solution-processed electronic[1−3] and optoelectronic devices.[4−8] Recently, localized surface plasmon resonance (LSPR) has been observed in cation-deficient copper chalcogenide nanocrystals (NCs).[9−13] The LSPR is due to collective oscillation of the free holes created by copper deficiency.[14] This differs from the LSPR observed in noble metal NCs[15,16] (i.e., Au and Ag) which is mediated by free electrons. Resonance between charge carrier oscillations and the frequency of incident light produces intense extinction bands at near-infrared (NIR) wavelengths.[13,17] This property opens up potential applications such as plasmonic optoelectronics devices,[18] sensors,[19] and theranostics.[19−21] The peak LSPR extinction wavelength in copper chalcogenide NCs depends upon the concentration of free holes, directly associated with the stoichiometry of the NCs. Lower Cu content (increasing Cu deficiency) produces a higher concentration of holes, resulting in an increase in the LSPR energy, i.e., a blue-shift of the wavelength of the LSPR extinction peak.[22] For anisotropic NCs, the LSPR wavelength also depends upon the aspect ratio.

Because the LSPR depends upon the doping level of the NCs, one may reasonably assume that catalytic activity of the NCs would be correlated with their LSPR. However, to the best of our knowledge, the electrocatalytic properties of such degenerately doped copper chalcogenide NCs have not yet been explored. Electrocatalysis is a subject of great recent interest due to its important role in fuel cells, electrolysis, and other energy storage and conversion technologies. In general, electrocatalytic activity depends strongly on charge transfer at electrode/electrolyte interfaces. Free hole-rich copper chalcogenides may provide a new opportunity to develop novel electrocatalysts. Motivated by this, we studied Cu-deficient $Cu_{2-x}S$ as an efficient catalyst for the oxygen reduction reaction (ORR), one of the most important reactions for a wide variety

Received: January 20, 2015
Revised: March 6, 2015
Published: March 12, 2015

DOI: 10.1021/acscatal.5b00115
ACS Catal. 2015, 5, 2534−2540

of electrochemical energy technologies such as polymer electrolyte fuel cells (PEFCs) and metal−air batteries (MABs).[23−26] Platinum has long been known as the most effective catalyst to facilitate the ORR in terms of its activity and stability, but its scarcity and high cost limit widespread implementation of these clean energy technologies.[26−28] Thus, development of alternative nonprecious metal catalysts is a key step toward broader adoption of these clean energy technologies. To date, the most promising nonprecious metal catalysts studied for the ORR are derived from Fe/Co, N, and C through a high-temperature approach.[29−33] However, their activity and stability are still insufficient.[34,35] Continued effort is still required to further explore new types of nonprecious metal catalysts.

Here, we provide the first demonstration that plasmonic copper sulfide ($Cu_{2-x}S$) NCs can serve as a highly active ORR electrocatalyst in alkaline media. Monodisperse colloidal $Cu_{2-x}S$ nanoplates with tunable LSPR were produced using a facile and scalable one-pot approach that does not require precursor injection at high temperature. The synthesis is tunable to optimize the electrochemical properties of the NCs. Notably, $Cu_{2-x}S$ is composed of relatively nontoxic, low-cost, and earth-abundant elements, and sulfur is preferred over the other chalcogenide elements on this basis. The band structures of the various possible crystal phases of $Cu_{2-x}S$ exhibit stoichiometry-dependent bandgap and Fermi level. During the colloidal synthesis, we focus on the inherent correlations among elemental composition, morphology, crystal phase, and optical properties. The LSPR energy is strongly influenced by the Cu:S precursor ratio used during the synthesis. In this study, the most heavily doped $Cu_{2-x}S$ nanoplates (lowest Cu content and highest LSPR energy) exhibited the best ORR activity. The electrochemical activity of $Cu_{2-x}S$ was further enhanced when the NCs were deposited on carbon black (Vulcan XC-72) or reduced graphene oxide (rGO). These results suggest that the Cu-deficient $Cu_{2-x}S$ can be a new class of nonprecious metal electrocatalysts for the ORR in alkaline media.

EXPERIMENTAL SECTION

Chemicals. Copper(I) chloride (CuCl, 99.995%), oleylamine (OAm,70%), sulfur (S) powder (99.98%), and trioctylphosphine oxide (TOPO, technical grade 90%) were purchased from Sigma-Aldrich and were used as-received.

One-Pot Synthesis of $Cu_{2-x}S$ Nanoplates. In a typical procedure, a selected quantity of CuCl (0.25, 0.375, or 0.5 mmol) was mixed with 1 mmol S powder, 4 g trioctylphosphine oxide (TOPO) and 10 mL oleylamine (OAm). The solution was degassed at room temperature under nitrogen protection followed by heating to 85 °C and maintaining this temperature for 1 h. After that, the heating mantle was removed and 20−30 mL ethanol was injected, reducing the temperature to ∼40 °C. $Cu_{2-x}S$ samples were collected by centrifugation at 9000 rpm (about 9000 G) for 1 min. The collected $Cu_{2-x}S$ samples were redispersed in chloroform. This procedure was repeated twice to purify the NCs. Finally, the resulting samples were dispersed in chloroform for subsequent characterization and tests.

Preparation of Carbon (C) Supported and Reduced Graphene Oxide (rGO) Supported $Cu_{2-x}S$ Nanoinks. Carbon black (Vulcan XC-72) was used to support the $Cu_{2-x}S$ nanoplates. In a typical procedure, 10 mg of carbon black was dispersed in 1.0 mL $Cu_{2-x}S$ (∼2 mg/mL) dispersion with 1.0 mL chloroform added and sonicated for 1 h at room temperature. The resulting dispersion was used to produce thin film electrodes with $Cu_{2-x}S$ content of 17 wt % for electrochemical measurements. Similarly, rGO supported $Cu_{2-x}S$ inks were produced by mixing 3.0 mg rGO (purchased from Graphene Supermarket with a surface area of 290 m^2/g), 0.3 mL $Cu_{2-x}S$ (∼2 mg/mL) dispersion, and 0.2 mL chloroform via sonication for 1 h at room temperature. This resulted in a final material with the same $Cu_{2-x}S$ content of ∼17 wt %.

Material Characterization. Transmission Electron Microscopy (TEM). The size and morphology of $Cu_{2-x}S$ NCs were characterized using a JEOL JEM-2010 microscope at a working voltage of 200 kV.

Powder X-ray Diffraction (XRD). The crystal phases of $Cu_{2-x}S$ NCs were determined using powder XRD (Rigaku Ultima IV with Cu K-α X-rays). Samples were prepared by drop-casting high-concentration $Cu_{2-x}S$ NC dispersions onto glass slides.

Energy Dispersive X-ray Spectroscopy. Compositional analysis of $Cu_{2-x}S$ NCs was obtained using an Oxford Instruments X-Max 20 mm^2 energy dispersive X-ray spectroscopy (EDS) detector within a Zeiss Auriga scanning electron microscope (SEM)

UV−vis-NIR Spectroscopy. Optical absorbance spectra of $Cu_{2-x}S$ NCs dispersions were measured using a Shimadzu 3600 UV−visible-NIR scanning spectrophotometer.

Electrochemical Measurements. To determine the electrocatalytic activity for the ORR, rotating disc electrode (RDE) measurements using $Cu_{2-x}S$ catalysts were performed in a conventional three-electrode cell with 0.1 M NaOH solution at room temperature. A graphite rod and an Ag/AgCl electrode (KCl-sat., 0.996 V vs RHE) were used as the counter and reference electrodes, respectively. The $Cu_{2-x}S$ or supported $Cu_{2-x}S$ was drop-cast onto a glassy carbon electrode (0.245 cm^2 area) and dried under a heating lamp to achieve an adherent film with the desired loading. The loading of $Cu_{2-x}S$ was controlled at 80 $\mu g/cm^2$ for all tests. For carbon black and rGO supported $Cu_{2-x}S$ catalysts, the loading of $Cu_{2-x}S$ was still kept at 80 $\mu g/cm^2$. In RDE tests, ORR steady-state polarization curves were recorded in oxygen-saturated 0.1 M NaOH solutions with potential steps of 0.03 V at intervals of 30 s. Disk rotation rates of 400, 900, 1600, and 2500 rpm were used. The Pt/C reference catalyst used in this work is 20 wt % E-TEK Pt/Vulcan XC-72.

RESULTS AND DISCUSSION

A facile synthetic method was developed to prepare monodisperse $Cu_{2-x}S$ nanocrystals (NCs) by heating copper salt and sulfur powder at a moderate temperature (∼85 °C) in a solution containing oleylamine and TOPO. To the best of our knowledge, no prior reports have used sulfur powder as the S donor during the one-pot synthesis of colloidal plasmonic copper sulfide NCs below 100 °C. Many previous reports of the synthesis of $Cu_{2-x}S$, used temperatures above 200 °C.[9,36] With elemental sulfur dissolved in oleic acid or oleylamine as the sulfur precursor, homogeneous $Cu_{2-x}S$ nanoparticles can be grown above 105 °C, following hot-injection at higher temperature, usually above 140 °C.[12,37] Other methods using dodecanethiol or ammonium diethyldithiocarbamate/dodecanethiol mixtures typically employ temperatures from 120 to 200 °C.[38−40]

Here, through our selection of precursors and ligands, we were able to synthesize copper sulfide NCs using moderate heating (<100 °C) of a mixture of CuCl, S, TOPO, and oleylamine. During heating, the color of the solution gradually turned to dark brown, indicating the nucleation and growth of NCs. During the low-temperature synthesis, the process of formation of organo-cation and organo-anion complexes and the NC nucleation can occur at the same time. Numerous previous studies succeeded in using organic molecules and appropriate precursors to achieve high quality NCs with tunable physical and chemical properties. Here, we demonstrate that the optical properties can be manipulated by varying the concentration of cations in the precursor mixture. Figure 1 shows TEM images of highly monodisperse $Cu_{2-x}S$ nanoplates obtained using 0.25, 0.375, and 0.5 mmol of CuCl in the

DOI: 10.1021/acscatal.5b00115
ACS Catal. 2015, 5, 2534−2540

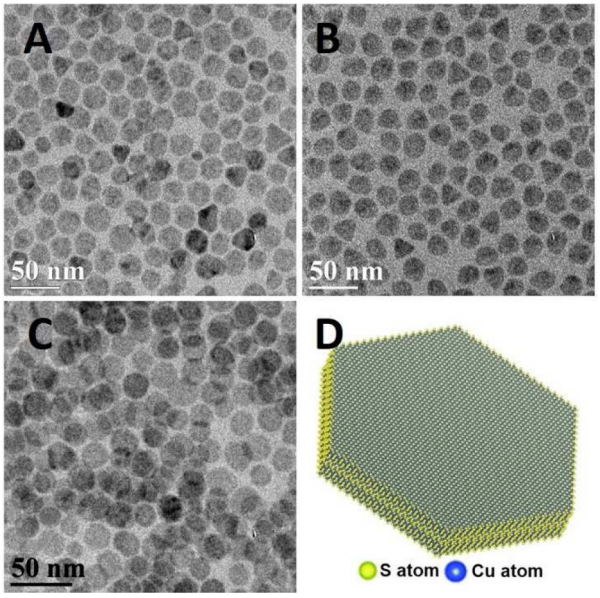

Figure 1. TEM images of $Cu_{2-x}S$ nanoplates synthesized using a one-pot method with varying Cu precursor amount. The CuCl used and resulting average diameter are (A) 0.25 mmol, 22.4 ± 2.4 nm; (B) 0.375 mmol, 21.2 ± nm; (C) 0.5 mmol, 21.4 ± 2.2 nm, respectively. (D) Ball-and-stick model of a $Cu_{2-x}S$ nanoplate of covellite crystal structure with diameter of ~20 nm and thickness of ~3 nm. Size distributions are shown in Supporting Information Figure S2. They are approximately Gaussian with the standard deviations given above.

synthesis, each with an average lateral diameter of ~21 nm. The size and morphology of the $Cu_{2-x}S$ nanoplates did not vary significantly with changes in the Cu precursor concentration. The thickness of nanoplates was in the range of 2.5−3.5 nm and nanoplates tended to assemble face-to-face into columns (Supporting Information Figure S1).

Energy dispersive X-ray spectroscopy (EDS) provided elemental composition of Cu and S in the final $Cu_{2-x}S$ nanoplates. The EDS results showed that the copper content in the final products decreased with increasing amount of CuCl supplied during the synthesis, from 0.25 to 0.5 mmol with a constant 1 mmol of sulfur. Figure 2A shows the relationship between the Cu cation faction in $Cu_{2-x}S$ and molar amount of CuCl used in the synthesis. In particular, the Cu content dropped 4.1% from 50.6% to 46.5% upon doubling the Cu

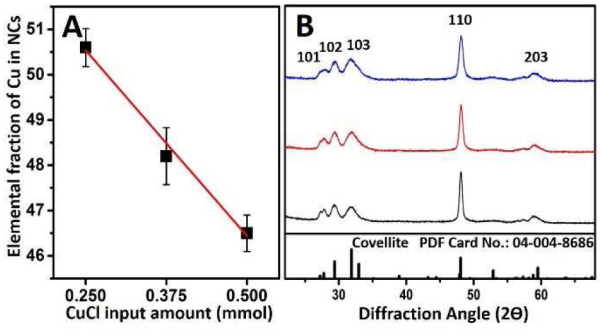

Figure 2. (A) Dependence of Cu content in $Cu_{2-x}S$ NCs upon the amount of CuCl precursor used in synthesis. (B) XRD patterns of $Cu_{2-x}S$ nanoplates synthesized using 0.25 mmol (black curve, bottom), 0.375 mmol (red curve, middle), and 0.5 mmol (blue curve, top) of CuCl.

precursor amount. Although this trend is somewhat counter-intuitive, one should note that in this single-pot method, precursor dissolution and complexation of Cu and S can occur simultaneously with nanoparticle nucleation and growth. Thus, while providing more CuCl produces a higher copper concentration in solution after all precursors have dissolved, it does not necessarily produce a higher Cu concentration in solution during initial stages of particle nucleation and growth when the CuCl has not yet fully dissolved. Although the mechanism behind this observation is not yet clear, and merits further study, it was consistently reproducible. Despite the changes in Cu content in $Cu_{2-x}S$, the platelike morphology and size remained unchanged. Figure 2B shows the XRD patterns of the $Cu_{2-x}S$ NCs as a function of the amount of CuCl provided. They were consistent with PDF card No. 04-004-8686 for hexagonal covellite. The main peaks were indexed to the (1 0 1), (1 0 2), (1 0 3), (1 1 0), and (2 0 3) planes. No obvious shift was detected upon increasing the amount of CuCl provided. The (1 1 0) peak was significantly sharper than other peaks, suggesting anisotropic growth of oriented plate- or disklike structures during this low temperature one-pot synthesis.[41] More detailed studies of the mechanism of anisotropic growth of metal sulfide NCs in this process are a promising area for future study.

UV−vis-NIR absorbance spectra were measured to characterize the LSPR in $Cu_{2-x}S$. Free holes in *p*-doped semiconductor NCs produce strong LSPR. The LSPR energy is directly dependent upon the free carrier concentration, which in turn depends upon the copper content. Several methods of tuning the plasmonic properties in those semiconductor NCs have been reported, including stepwise oxidization−reduction,[42,43] tuning the aspect ratio of anisotropic nanostructures,[44] cation exchange,[10,45] and manipulating the surface chemistry of NCs.[12,13] Here, we found that the LSPR in these copper sulfide nanoplates is tunable by simply changing the amount of CuCl provided during the one-pot synthesis. To confirm that the observed absorbance arises from LSPR, we tested its dependence upon the refractive index of the NC's surroundings. Figure 3A shows a red-shift of the NIR absorbance with increasing refractive index of the solvent in which $Cu_{2-x}S$ were dispersed. The peak of the LSPR absorbance was red-shifted nearly 150 nm from hexane to carbon disulfide. This red-shift of absorbance with increasing refractive index of the solvent is a hallmark behavior of LSPR. The resonance in polarizability of the NC is associated with the relative dielectric constants of the

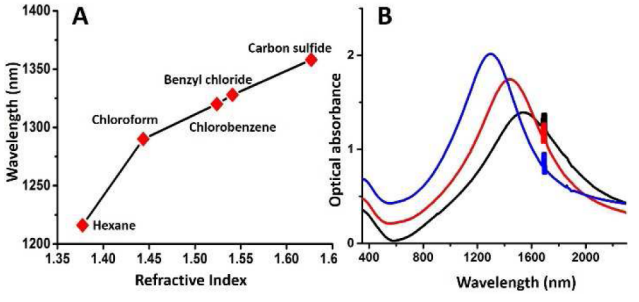

Figure 3. Optical properties of $Cu_{2-x}S$ NCs. (A) Dependence of LSPR absorbance peak wavelength on solvent refractive index for $Cu_{2-x}S$ NCs synthesized using a 0.5 mmol Cu precursor. (B) Absorbance spectra of $Cu_{2-x}S$ NCs synthesized using Cu precursor input amounts of 0.5 mmol (blue curve), 0.375 mmol (red curve), and 0.25 mmol (black curve), in $CHCl_3$.

DOI: 10.1021/acscatal.5b00115
ACS Catal. 2015, 5, 2534−2540

NC and the surroundings.[9,22] Meanwhile, as shown in Figure 3B, the $Cu_{2-x}S$ sample synthesized using 0.5 mmol Cu precursor shows a dominant LSPR peak at 1290 nm, in chloroform. Upon reducing the CuCl amount from 0.5 to 0.375 and 0.25 mmol, the LSPR peak red-shifted to 1450 and 1540 nm, respectively. Thus, by varying the amount of CuCl provided during the synthesis of copper sulfide NCs, we can easily tune the plasmonic properties and manipulate the doping level of the particles. XRD and TEM studies further indicated that the crystal structure, morphology, and size of $Cu_{2-x}S$ nanoplates were independent of copper precursor amount. However, because the Cu content decreased with increasing amount of CuCl provided, the free carrier concentration increased, resulting in a blue shift of the LSPR. This provides a straightforward new means of adjusting the concentration of free holes in these NCs.

Because electrocatalytic performance for the ORR depends upon charge transfer at the electrode/electrolyte interface, correlation of electrocatalytic activity with LSPR wavelength and corresponding concentration of free holes is of interest. To this end, $Cu_{2-x}S$ nanoplates were systematically studied as an electrocatalyst for the ORR in alkaline solution. $Cu_{2-x}S$ nanoplates were drop-deposited as thin films on the surface of glassy carbon electrodes at a constant mass loading (80 μg/cm^2). ORR steady-state polarization plots for each sample of $Cu_{2-x}S$ nanoplates were recorded at a rotation rate of 900 rpm and room temperature, are shown in Figure 4A. The $Cu_{2-x}S$ catalyst synthesized using 0.5 mmol Cu precursor ($Cu_{2-x}S$-0.5) showed the best activity, compared to samples prepared using 0.25 ($Cu_{2-x}S$-0.25) and 0.375 mmol ($Cu_{2-x}S$-0.375), as evidenced by the most positive half-wave potential ($E_{1/2}$) of 0.70 V. Lower $E_{1/2}$ of 0.64 and 0.62 V were measured with $Cu_{2-x}S$-0.375 and $Cu_{2-x}S$-0.25, respectively. In addition, the onset potential of the ORR for $Cu_{2-x}S$-0.5 was as high as 0.90 V, which is much more positive than those of $Cu_{2-x}S$-0.375 (0.85 V) and $Cu_{2-x}S$-0.250 (0.75 V). This suggests that the nature of the active sites is changed due to the increased copper deficiency. According to EDS and plasmonic peak analysis, $Cu_{2-x}S$ NCs derived from 0.5 mmol Cu precursor were the most heavily doped. Given the nearly identical crystal structures, morphologies, and sizes for the three samples, the much increased catalytic activity measured with the $Cu_{2-x}S$-0.5 sample is attributed to its significantly higher concentration of free holes, likely providing more active sites for the ORR. To the best of our knowledge, this is the first report using metal deficient plasmonic sulfide NCs as an efficient electrocatalyst for the ORR.

In order to further improve the electrocatalytic performance by enhancing electrical conductivity and utilization of active catalysts, the $Cu_{2-x}S$ nanoplates were deposited on Vulcan XC-72 carbon black and rGO through a self-assembly approach in solution. Figure 5 shows typical TEM images of the $Cu_{2-x}S$-0.5 NCs anchored on Vulcan XC-72 (Figure 5A, C−$Cu_{2-x}S$) and rGO (Figure 5B, rGO-$Cu_{2-x}S$). The $Cu_{2-x}S$ NCs self-assembled onto both carbon supports during mild sonication in chloroform solution. Steady-state RDE measurements were then carried out to study ORR activity and kinetics on C−$Cu_{2-x}S$ and rGO-$Cu_{2-x}S$ catalysts. Figure 4B shows typical polarization curves recorded in O_2-saturated 0.1 M NaOH solution at a rotation rate of 900 rpm and room temperature. Compared to $Cu_{2-x}S$ alone, both carbon supported C−$Cu_{2-x}S$ and rGO-$Cu_{2-x}S$ exhibit dramatically increased current densities in the kinetic potential region, with well-defined

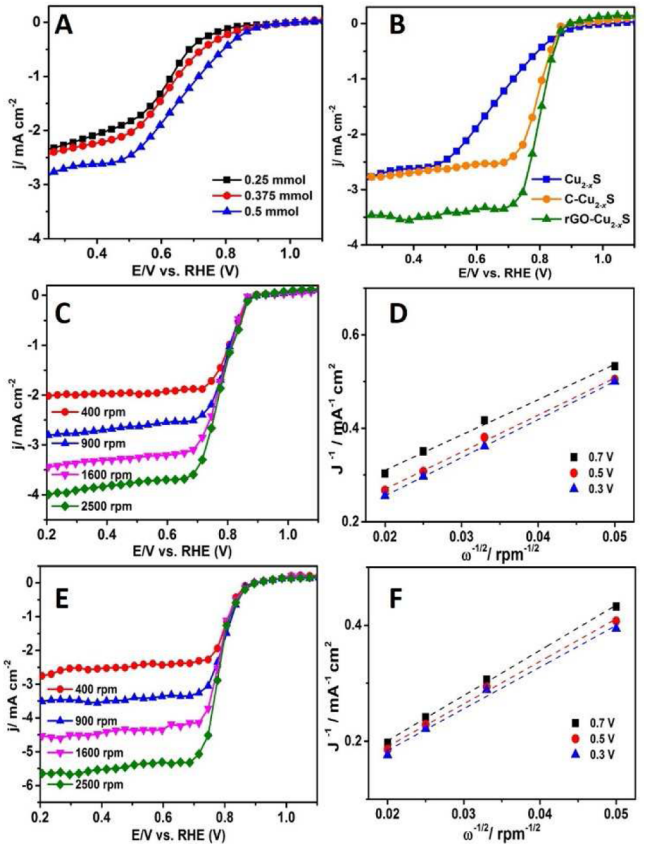

Figure 4. (A) ORR steady-state polarization curves of $Cu_{2-x}S$ NCs synthesized using 0.25, 0.375, and 0.5 mmol Cu precursors. (B) steady-state polarization curves for $Cu_{2-x}S$ NCs, C−$Cu_{2-x}S$, and rGO-$Cu_{2-x}S$. (C and E) ORR steady-state polarization curves for C−$Cu_{2-x}S$ (C) and rGO-$Cu_{2-x}S$ (E) with varying electrode rotation rates. (D and F) Koutecky−Levich plots of the ORR for C−$Cu_{2-x}S$ (D) and rGO-$Cu_{2-x}S$ (F). The measurements were performed in O_2-saturated NaOH (0.1 M) solution.

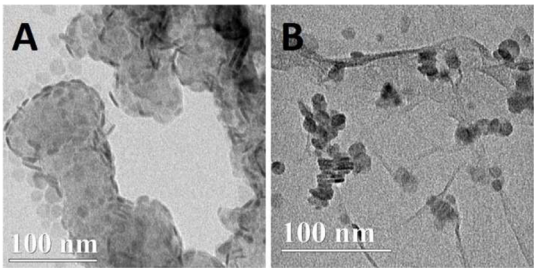

Figure 5. TEM images of $Cu_{2-x}S$ nanoplates deposited on carbon black (C−$Cu_{2-x}S$, A) and reduced graphene oxide (rGO-$Cu_{2-x}S$, B).

limiting currents. Both supported catalysts showed more positive half-wave potentials $E_{1/2}$ (C−$Cu_{2-x}S$ 0.80 V, rGO-$Cu_{2-x}S$ 0.82 V), relative to $Cu_{2-x}S$ NCs alone (0.70 V). This indicates that using XC-72 carbon black or rGO as the catalyst support leads to a significant increase in the number of active sites for the ORR. Importantly, the degree of activity improvement using rGO was greater than that using XC-72 as the support, as evidenced by more positive half-wave potential and larger limiting currents. As discussed in previous reports,[30,46,47] the advantages of reduced graphene oxide (rGO) for electrocatalysis arise from its high-surface area, excellent electrical conductivity, electrochemical stability, and unique

DOI: 10.1021/acscatal.5b00115
ACS Catal. 2015, 5, 2534−2540

two-dimensional planar morphology.[31] We also studied the catalytic activity of the Vulcan XC-72 and rGO without Cu_{2-x}NCs, as shown in Figure S4. These supports had much lower activity relative to the C−Cu_{2-x}S or rGO-Cu_{2-x}S. This result confirms that the significant enhancement of rGO-Cu_{2-x}S is derived from the remarkable support effect of rGO and not from any intrinsic electrocatalytic activity of the rGO itself. In addition, the limiting current density for the ORR was increased when rGO was used for supporting Cu_{2-x}S nanocrystals. Although the limiting current density of planar disk electrodes is theoretically governed by rotation rate during the ORR experiments, based on the Koutecky−Levich equation, an increasing body of evidence shows that increased porous structures and surface areas of electrodes play an important role in enhancing limiting current.[48] In this work, the high surface area and excellent electrical conductivity of graphene (rGO) lead to significantly enhanced limiting currents, relative to unsupported Cu_{2-x}S nanocrystals. Thus, the high activity for the ORR measured with the rGO-Cu_{2-x}S not only originates from heavily *p*-doped Cu_{2-x}S but is also further enhanced by the unique rGO support effect.

Furthermore, the electrocatalytic activity for the C−Cu_{2-x}S and rGO-Cu_{2-x}S were quantitatively examined at several electrode rotation rates of 400, 900, 1600, and 2500 rpm. Figure 4C and E shows the rotation-speed controlled current densities of the ORR measured with the C−Cu_{2-x}S and rGO-Cu_{2-x}S catalysts, respectively. The corresponding Koutecky−Levich (K−L) plots as a function of different ORR working potentials are shown in parts D and F, with a correlation between the inverse current density (j^{-1}) and the inverse of the square root of rotation rate ($\omega^{-1/2}$). The number of electrons involved per O_2 reduction on carbon supported Cu_{2-x}S catalysts was calculated according to the modified K−L equation for a film-coated electrode.[49] As a result, the number of electrons *n* calculated for rGO-Cu_{2-x}S is 3.67−3.98, which is slightly larger than that for C−Cu_{2-x}S (3.50−3.78), thereby suggesting a four-electron ($4e^-$) O_2 reduction process to OH^-. The calculated electron transfer numbers are in good agreement with the measured low peroxide yield as shown in Figure 6. Thus, compared to C−Cu_{2-x}S, rGO-Cu_{2-x}S not only generated a higher current density but is also more favorable for efficient oxygen reduction to OH^-, rather than peroxide.

The best performing rGO-Cu_{2-x}S catalysts were further compared with the state-of-the-art carbon supported platinum (C−Pt). In this comparison, two different Pt standard loadings of 20 and 60 $\mu g/cm^2$ were used as shown in Figure 7. At this

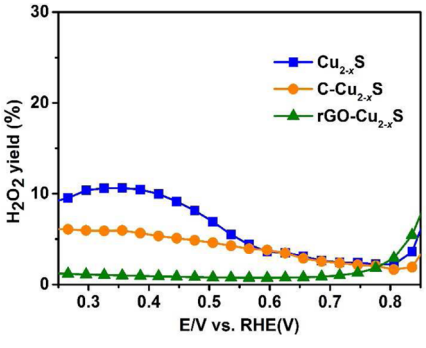

Figure 6. H_2O_2 yield measured with the Cu_{2-x}S, C−Cu_{2-x}S, and rGO-Cu_{2-x}S catalysts in O_2-saturated 0.1 M NaOH at room temperature with rotation rate of 900 rpm.

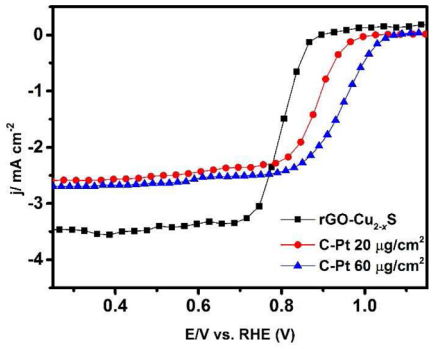

Figure 7. Polarization curves measured in 0.1 M NaOH solution (room temperature, 900 rpm) for rGo-Cu_{2-x}S and C−Pt. The loading of Pt was 20 $\mu g/cm^2$ (red curve) or 60 $\mu g/cm^2$ (blue curve).

point, the catalytic activity of rGO-Cu_{2-x}S is still inferior to that of C−Pt catalysts. However, this work provides a new route to develop nonprecious metal catalysts by tuning the concentration of free holes in degenerately *p*-doped Cu_{2-x}S resulting from cation vacancies. This is significantly different from the extensively studied conventional M−N−C (M: Fe or Co) nonprecious metal catalysts.[27]

To provide further mechanistic understanding of the ORR on this new type of Cu-deficient Cu_{2-x}S catalysts, Tafel plots were constructed as shown in Figure 8. According to the K−L

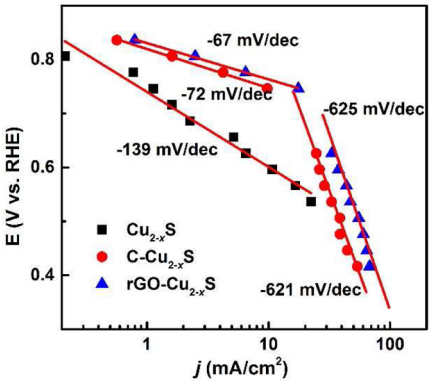

Figure 8. Tafel plots for the ORR on Cu_{2-x}S, C−Cu_{2-x}S, and rGO-Cu_{2-x}S.

equation, the ORR kinetic current densities were calculated from the steady-state polarization and used to prepare these Tafel plots. Oxygen reduction in alkaline electrolyte involves multiple steps due to many possible intermediate species, such as O, OH, O_2^-, and HO_2^-. In theory, the rate-determining step (RDS) associated with the first-electron transfer yields a Tafel slope of −118 mV/dec. Oppositely, a Tafel slope of −59 mV/dec is due to a migration of adsorbed oxygen intermediates on catalysts, resulting from a coverage-dependent activation barrier for the ORR.[48,50] Here, the standalone Cu_{2-x}S catalysts exhibited a Tafel slope of −139 mV/dec, suggesting that the first electron transfer during the ORR is likely the slowest step, thereby limiting the overall reaction rates. When carbon supports (XC-72 and rGO) were used to support Cu_{2-x}S, charge transfer is significantly enhanced, showing different Tafel slopes. Both XC-72 and rGO supported Cu_{2-x}S catalysts have similar Tafel slopes. This implies that choice of carbon supports used to enhance catalytic activity does not affect the reaction mechanism. Notably, two well-defined Tafel regions

DOI: 10.1021/acscatal.5b00115
ACS Catal. 2015, 5, 2534−2540

were simulated for these carbon supported $Cu_{2-x}S$ catalysts, with a transition from ca. −70 mV/dec (E > 0.73 V) to ca. −620 mV/dec (E < 0.73 V). The Tafel slope of 70 mV/dec at high potential range is between −120 and −59 mV/dec, suggesting that oxygen reduction on carbon supported $Cu_{2-x}S$ catalysts is controlled simultaneously by charge transfer and intermediate migration. At lower potential, the high Tafel slope values suggest that O_2 adsorption onto catalytic sites becomes the RDS.[51,52]

CONCLUSION

In this work, we have demonstrated a facile one-pot method to synthesize Cu-deficient $Cu_{2-x}S$ nanoplates with tunable plasmonic properties. The amount of copper precursor supplied was shown to control the copper content and therefore the free hole concentration and LSPR energy at fixed NC size and shape. The newly developed synthesis method only requires moderate heating (∼85 °C) of a copper salt and sulfur powder in oleylamine/TOPO solution. The resulting $Cu_{2-x}S$ nanoplates were shown to serve as active electrocatalysts for the ORR in alkaline electrolyte. When $Cu_{2-x}S$ nanoplates were supported on reduced graphene oxide, a substantial enhancement of activity was achieved, compared to $Cu_{2-x}S$ alone, due to improved electrical conductivity and utilization of active species, along with a very likely synergistic effect between the $Cu_{2-x}S$ and graphene.[53] Further understanding of the nature of active sties at the atomic level will be gained using first principle calculations and advanced spectroscopic characterization, which will be the subject of future studies. Although the electrocatalytic activity achieved with these first $Cu_{2-x}S$ catalysts is still inferior to the state-of-the-art C−Pt catalysts, this research may open up a new route to develop alternative nonprecious metal catalysts by exploring the novel free-hole-rich Cu-deficient sulfides.

ASSOCIATED CONTENT

Supporting Information

The following file is available free of charge on the ACS Publications website at DOI: 10.1021/acscatal.5b00115.

Additional TEM images, size distributions of NCs, steady-state polarization plots for support materials without $Cu_{2-x}S$ NCs (PDF)

AUTHOR INFORMATION

Corresponding Authors

*E-mail: swihart@buffalo.edu (M.T.S.).
*E-mail: gangwu@buffalo.edu (G.W.).

Notes

The authors declare no competing financial interest.

ACKNOWLEDGMENTS

The authors gratefully acknowledge financial support from the New York State Center of Excellence in Materials Informatics (M.T.S.) and startup funds from the University at Buffalo (SUNY) (G.W.).

REFERENCES

(1) Riha, S. C.; Johnson, D. C.; Prieto, A. L. *J. Am. Chem. Soc.* **2010**, *133*, 1383−1390.
(2) Qian, X.; Liu, H.; Chen, N.; Zhou, H.; Sun, L.; Li, Y.; Li, Y. *Inorg. Chem.* **2012**, *51*, 6771−6775.
(3) Devulder, W.; Opsomer, K.; Seidel, F.; Belmonte, A.; Muller, R.; De Schutter, B.; Bender, H.; Vandervorst, W.; Van Elshocht, S.; Jurczak, M. *ACS Appl. Mater. Interfaces* **2013**, *5*, 6984−6989.
(4) Lee, H.; Yoon, S. W.; Kim, E. J.; Park, J. *Nano Lett.* **2007**, *7*, 778−784.
(5) Wu, Y.; Wadia, C.; Ma, W.; Sadtler, B.; Alivisatos, A. P. *Nano Lett.* **2008**, *8*, 2551−2555.
(6) Pan, C.; Niu, S.; Ding, Y.; Dong, L.; Yu, R.; Liu, Y.; Zhu, G.; Wang, Z. L. *Nano Lett.* **2012**, *12*, 3302−3307.
(7) Riha, S. C.; Jin, S.; Baryshev, S. V.; Thimsen, E.; Wiederrecht, G. P.; Martinson, A. B. *ACS Appl. Mater. Interfaces* **2013**, *5*, 10302−10309.
(8) Wang, F.; Dong, H.; Pan, J.; Li, J.; Li, Q.; Xu, D. *J. Phys. Chem. C* **2014**, *118*, 19589−19598.
(9) Comin, A.; Manna, L. *Chem. Soc. Rev.* **2014**, *43*, 3957−3975.
(10) Wang, X.; Liu, X.; Zhu, D.; Swihart, M. T. *Nanoscale* **2014**, *6*, 8852−8857.
(11) Zhao, Y.; Burda, C. *Energy Environ. Sci.* **2012**, *5*, 5564−5576.
(12) Liu, X.; Wang, X.; Zhou, B.; Law, W. C.; Cartwright, A. N.; Swihart, M. T. *Adv. Funct. Mater.* **2013**, *23*, 1256−1264.
(13) Liu, X.; Wang, X.; Swihart, M. T. *Chem. Mater.* **2013**, *25*, 4402−4408.
(14) Luther, J. M.; Jain, P. K.; Ewers, T.; Alivisatos, A. P. *Nat. Mater.* **2011**, *10*, 361−366.
(15) Zhang, C.; Yin, A.-X.; Jiang, R.; Rong, J.; Dong, L.; Zhao, T.; Sun, L.-D.; Wang, J.; Chen, X.; Yan, C.-H. *ACS Nano* **2013**, *7*, 4561−4568.
(16) Gao, C.; Hu, Y.; Wang, M.; Chi, M.; Yin, Y. *J. Am. Chem. Soc.* **2014**, *136*, 7474−7479.
(17) Xie, Y.; Riedinger, A.; Prato, M.; Casu, A.; Genovese, A.; Guardia, P.; Sottini, S.; Sangregorio, C.; Miszta, K.; Ghosh, S. *J. Am. Chem. Soc.* **2013**, *135*, 17630−17637.
(18) Niezgoda, J. S.; Yap, E.; Keene, J. D.; McBride, J. R.; Rosenthal, S. J. *Nano Lett.* **2014**, *14*, 3262−3269.
(19) Li, W.; Zamani, R.; Rivera Gil, P.; Pelaz, B.; Ibáñez, M.; Cadavid, D.; Shavel, A.; Alvarez-Puebla, R. A.; Parak, W. J.; Arbiol, J. *J. Am. Chem. Soc.* **2013**, *135*, 7098−7101.
(20) Liu, X.; Law, W. C.; Jeon, M.; Wang, X.; Liu, M.; Kim, C.; Prasad, P. N.; Swihart, M. T. *Adv. Healthcare Mater.* **2013**, *2*, 952−957.
(21) Hessel, C. M.; P. Pattani, V.; Rasch, M.; Panthani, M. G.; Koo, B.; Tunnell, J. W.; Korgel, B. A. *Nano Lett.* **2011**, *11*, 2560−2566.
(22) Liu, X.; Swihart, M. T. *Chem. Soc. Rev.* **2014**, *43*, 3908−3920.
(23) Wu, G.; Nelson, M. A.; Mack, N. H.; Ma, S.; Sekhar, P.; Garzon, F. H.; Zelenay, P. *Chem. Commun.* **2010**, *46*, 7489−7491.
(24) Bing, Y.; Liu, H.; Zhang, L.; Ghosh, D.; Zhang, J. *Chem. Soc. Rev.* **2010**, *39*, 2184−2202.
(25) Wu, G.; More, K. L.; Johnston, C. M.; Zelenay, P. *Science* **2011**, *332*, 443−447.
(26) Li, Q.; Cao, R.; Cho, J.; Wu, G. *Phys. Chem. Chem. Phys.* **2014**, *16*, 13568−13582.
(27) Wu, G.; Zelenay, P. *Acc. Chem. Res.* **2013**, *46*, 1878−1889.
(28) Li, Q.; Cao, R.; Cho, J.; Wu, G. *Adv. Energy Mater.* **2014**, *4*, 1301415.
(29) Wu, G.; More, K. L.; Xu, P.; Wang, H.-L.; Ferrandon, M.; Kropf, A. J.; Myers, D. J.; Ma, S.; Zelenay, P. *Chem. Commun.* **2013**, *49*, 3291−3293.
(30) Li, Q.; Xu, P.; Gao, W.; Ma, S.; Zhang, G.; Cao, R.; Cho, J.; Wang, H.-L.; Wu, G. *Adv. Mater.* **2014**, *26*, 1378−1386.
(31) Li, Q.; Wu, G.; Cullen, D. A.; More, K. L.; Mack, N. H.; Chung, H.; Zelenay, P. *ACS Catal.* **2014**, *4*, 3193−3200.
(32) Wu, G.; Mack, N. H.; Gao, W.; Ma, S.; Zhong, R.; Han, J.; Baldwin, J. K.; Zelenay, P. *ACS Nano* **2012**, *6*, 9764−9776.
(33) Wu, G.; Nelson, M.; Ma, S.; Meng, H.; Cui, G.; Shen, P. K. *Carbon* **2011**, *49*, 3972−3982.
(34) Li, Q.; Pan, H.; Higgins, D.; Cao, R.; Zhang, G.; Lv, H.; Wu, K.; Cho, J.; Wu, G. *Small* **2014**, DOI: 10.1002/smll.201402069.
(35) Wu, G.; Dai, C.; Wang, D.; Li, D.; Li, N. *J. Mater. Chem.* **2010**, *20*, 3059−3068.

DOI: 10.1021/acscatal.5b00115
ACS Catal. 2015, 5, 2534−2540

(36) Saldanha, P. L.; Brescia, R.; Prato, M.; Li, H.; Povia, M.; Manna, L.; Lesnyak, V. *Chem. Mater.* **2014**, *26*, 1442−1449.
(37) Wang, X.; Swihart, M. T. *Chem. Mater.* **2015**, *27*, 1786−1791.
(38) Han, W.; Yi, L.; Zhao, N.; Tang, A.; Gao, M.; Tang, Z. *J. Am. Chem. Soc.* **2008**, *130*, 13152−13161.
(39) Kruszynska, M.; Borchert, H.; Bachmatiuk, A.; Rümmeli, M. H.; Büchner, B.; Parisi, J. r.; Kolny-Olesiak, J. *ACS Nano* **2012**, *6*, 5889−5896.
(40) Wu, Y.; Wadia, C.; Ma, W.; Sadtler, B.; Alivisatos, A. P. *Nano Lett.* **2008**, *8*, 2551−2555.
(41) Du, Y.; Yin, Z.; Zhu, J.; Huang, X.; Wu, X.-J.; Zeng, Z.; Yan, Q.; Zhang, H. *Nat. Commun.* **2012**, *3*, 1177.
(42) Dorfs, D.; Härtling, T.; Miszta, K.; Bigall, N. C.; Kim, M. R.; Genovese, A.; Falqui, A.; Povia, M.; Manna, L. *J. Am. Chem. Soc.* **2011**, *133*, 11175−11180.
(43) Kriegel, I.; Jiang, C.; Rodríguez-Fernández, J.; Schaller, R. D.; Talapin, D. V.; Da Como, E.; Feldmann, J. *J. Am. Chem. Soc.* **2012**, *134*, 1583−1590.
(44) Hsu, S.-W.; On, K.; Tao, A. R. *J. Am. Chem. Soc.* **2011**, *133*, 19072−19075.
(45) De Trizio, L.; Li, H.; Casu, A.; Genovese, A.; Sathya, A.; Messina, G. C.; Manna, L. *J. Am. Chem. Soc.* **2014**, *136*, 16277−16284.
(46) Li, Q.; Xu, P.; Zhang, B.; Tsai, H.; Wang, J.; Wang, H.-L.; Wu, G. *Chem. Commun.* **2013**, *49*, 10838−10840.
(47) He, Q.; Li, Q.; Khene, S.; Ren, X.; Bueno-López, A.; Wu, G. *J. Phys. Chem. C* **2013**, *117*, 8697−8707.
(48) Wu, G.; Chung, H. T.; Nelson, M.; Artyushkova, K.; More, K. L.; Johnston, C. M.; Zelenay, P. *ECS Trans.* **2011**, *41*, 1709−1717.
(49) Wu, G.; Cui, G.; Li, D.; Shen, P.-K.; Li, N. *J. Mater. Chem.* **2009**, *19*, 6581−6589.
(50) Wu, G.; Li, L.; Xu, B.-Q. *Electrochim. Acta* **2004**, *50*, 1−10.
(51) Li, Q.; Xu, P.; Zhang, B.; Tsai, H.; Zheng, S.; Wu, G.; Wang, H.-L. *J. Phys. Chem. C* **2013**, *117*, 13872−13878.
(52) Radyushkina, K.; Tarasevich, M. *Elektrokhimiya* **1970**, *6*, 1703−1705.
(53) Liang, Y.; Li, Y.; Wang, H.; Zhou, J.; Wang, J.; Regier, T.; Dai, H. *Nat. Mater.* **2011**, *10*, 780−786.

DOI: 10.1021/acscatal.5b00115
ACS Catal. 2015, 5, 2534−2540